

PREDICTION OF CORROSION OF NICKEL-BASE ALLOYS AND STAINLESS STEELS IN OXIDIZING ENVIRONMENTS USING THERMODYNAMIC AND ELECTROCHEMICAL MODELS

A. Anderko
OLI Systems, Inc.
108 American Road
Morris Plains, NJ 07950

N. Sridhar and C.S. Brossia
Southwest Research Institute
6220 Culebra Road
San Antonio, TX 78238

ABSTRACT

A comprehensive computational system has been developed for predicting long-term general and localized corrosion of Fe-Ni-Cr-Mo-W alloys in complex aqueous environments. The system relies on the computation of the corrosion and repassivation potentials as functions of solution chemistry and temperature. The corrosion potential is calculated from a mixed-potential model that combines comprehensive thermodynamic speciation calculations with a detailed treatment of partial electrochemical processes that may occur on the metal surface. The mixed-potential model has been verified by calculating corrosion rates in mixed acids and corrosion potential as a function of pH and concentration of oxidizing species. The repassivation potential is calculated from a separate model that quantitatively considers competitive processes at metal/salt film/solution interfaces in the limit of repassivation. This model has been shown to be accurate for reproducing the repassivation potential for mixtures containing both aggressive and inhibitive ions. Furthermore, a generalized correlation has been established to relate the repassivation potential to alloy composition. The combined predictive methodology has been validated by calculating the critical crevice temperature for a number of nickel-base alloys.

Keywords: Localized corrosion, acid corrosion, repassivation potential, corrosion potential, critical crevice temperature, modeling

INTRODUCTION

Localized corrosion is an extremely complex phenomenon that is influenced by diverse factors including the properties of chemical species in an aqueous environment, concentrations of components, alloy composition and temperature. In the last three decades, considerable progress was made in understanding the initiation, growth and repassivation of localized corrosion of various metallic materials.¹⁻⁶ Several modeling approaches to localized corrosion have been developed by considering atomic/molecular processes^{7,8}, microstructural features^{1,9} and transport processes in macroscopic cavities.¹⁰⁻¹³ These models have successfully contributed to our understanding of various aspects of pitting and crevice corrosion.

In previous papers,^{14,15} a different computational model has been proposed to predict the tendency of metals to undergo localized corrosion as a function of environmental conditions. This approach essentially divides the task of predicting localized corrosion into two parts, i.e., (1) calculating the corrosion potential and (2) predicting the repassivation potential, also called the protection potential. The repassivation potential (E_{rp}) is a measure of the tendency of an alloy to undergo localized corrosion in a given environment. The underlying justification for the use of E_{rp} is the fact that, for engineering applications, only the fate of stable pits or crevice corrosion is important. Pits that nucleate, but do not grow beyond an embryonic stage (metastable pits) do not adversely affect the performance of engineering structures. It has been shown in previous papers¹⁵⁻¹⁷ that (i) E_{rp} is the potential below which stable pitting or crevice corrosion does not occur and (ii) it is relatively insensitive to prior pit depth and surface finish. The predicted repassivation is then compared to the corrosion potential (E_{corr}) in the same environment to determine the alloy's susceptibility to localized corrosion. The separation of localized corrosion modeling into two steps is valid as long as the initiation of stable localized corrosion is being considered because the corrosion potential is not affected at this stage by the localized corrosion processes and the interaction between pits can be ignored. However, such a separation is not valid once significant pit or crevice corrosion growth occurs.

The concept is illustrated schematically in Figure 1. For a given alloy, the repassivation potential decreases with an increase in chloride concentration (cf. Figure 1a). In the general case, the main regions of the E_{rp} versus chloride concentration plot are a low-slope portion at high chloride concentrations and a high-slope portion at low concentrations. On the other hand, the corrosion potential is not a strong function of chloride concentration unless significant localized corrosion occurs. The critical chloride concentration for localized corrosion is observed when E_{corr} exceeds E_{rp} (Fig. 1a). Similarly, for a given chloride concentration, a critical temperature exists (Figure 1b). The repassivation potential is also strongly affected by the presence of inhibitors. As shown in Figure 1c, this gives rise to a critical inhibitor concentration. In many environments, the presence of oxidants may increase E_{corr} so that localized corrosion may occur beyond a critical concentration of redox species (Figure 1d). The actual conditions in a system may be a combination of the idealized cases shown in Figure 1a-d.

In this study, we demonstrate the applicability of this approach to several corrosion resistant alloys in various oxidizing environments. First, we apply a recently developed general corrosion model to calculate both corrosion rates and corrosion potentials of nickel-base alloys. In particular, the model is used to analyze the effects of pH, dissolved oxygen, nitrates, and other oxidants on the corrosion potential. Then, we use a separate model for calculating the repassivation potential for alloys in chloride-nitrate environments. Finally, we combine the E_{corr} and E_{rp} models to predict the critical crevice temperature, which provides a stringent test of the modeling approach.

EXPERIMENTAL PROCEDURES

The nominal chemical compositions of the alloys discussed in this paper are shown in Table 1. The corrosion rates in nitric, sulfuric acids and their mixtures were measured using non-creviced samples and weight-loss method. The exposure time for these tests ranged from 24 hours for sulfuric acid to 240 hours for nitric acid. The experimental procedures for measuring repassivation potentials were described previously.^{14,15} The crevice corrosion repassivation potential was obtained using specimens fitted with a serrated crevice washer made of polytetrafluoroethylene (PTFE). The crevice and pitting repassivation potentials are used interchangeably because they have been found to be equivalent for deep pits. Crevices were created on 3 mm thick sheet samples by clamping serrated PTFE washers (12 teeth per side) using alloy C-276 (UNS N10276) bolts isolated through PTFE sleeves at an initial torque of 0.14 N·m. The samples were held potentiostatically at a more positive potential such that the current density increased with time at this potential, which was indicative of localized corrosion growth. After a fixed charge density were passed at high potentials, the potential was lowered at a slow scan rate of 0.167 mV/s. The repassivation potentials were defined as potentials at which the current density corresponded to 10^{-2} A/m². The corrosion potentials were measured in static solutions on non-creviced specimens. For most measurements, a non-pitting background electrolyte (Na₂SO₄) was used.

COMPUTATIONAL MODEL

Computation of the corrosion potential

The corrosion potential is calculated using a previously developed general corrosion model (Anderko and Young,¹⁸ Anderko et al.¹⁹ and Sridhar et al.²⁰). The model was described in detail in previous papers¹⁸⁻²⁰ and, therefore, only a general outline is given here.

The model consists of a thermophysical module and an electrochemical module. The thermophysical module predicts the speciation of the aqueous environment and the activities and transport properties of solution species that participate in interfacial reactions (Rafal et al.,²¹ Anderko and Lencka²², Lencka et al.²³) The electrochemical model utilizes this information to simulate electrochemical reactions at the metal-solution interface. The electrochemical model of general corrosion takes into account various partial reactions on the surface of the metal and transport processes for the species that participate in the reactions. The model includes passivation phenomena, which may be influenced by pH and the presence of aggressive or inhibitive species in the solution. Further, it combines the partial processes to compute corrosion rates in the framework of the mixed potential theory.

The model includes expressions for partial anodic and cathodic processes, which may occur under activation or mass transport control. The expressions are in agreement with the generally accepted views on the mechanisms of partial processes. In the active state, the current density of metal dissolution is generally given by

$$i_{Me} = i_{Me}^0 \exp\left[\frac{\alpha_{Me} F (E - E_{Me}^0)}{RT}\right] \quad (1)$$

where the exchange current density i_{Me}^0 incorporates the effect of adsorption of species and is related to the activities of solution species as described in previous papers.¹⁸⁻²⁰

The active-passive transition is introduced into the electrochemical model by considering a current that leads to the formation of a passive layer in addition to the current that leads to active dissolution. At any instant, a certain fraction of the surface θ_p is assumed to be covered by a passive layer. The change of the passive layer coverage fraction with time is expressed as¹⁸

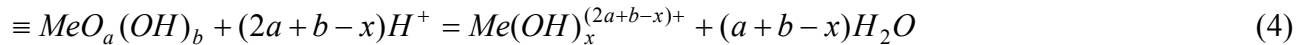
$$\left(\frac{\partial \theta_p}{\partial t}\right)_{E,a_i} = ci_{MeO}(1 - \theta_p) - K\theta_p \quad (2)$$

where i_{MeO} is the current density that contributes to the formation of a passive layer. The second term on the right-hand side of eq. (2) represents the rate of dissolution of the passive layer, which is proportional to the coverage fraction. Solution of this equation in the steady-state limit yields an expression for the anodic dissolution current:

$$i_{Me,TOT} = \frac{i_{Me} + i_{MeO}}{1 + \frac{ci_{MeO}}{K}} = \frac{i_{Me} + i_{MeO}}{1 + \frac{i_{MeO}}{i_p}} \quad (3)$$

where i_{Me} is the dissolution current density in the active state and the ratio $i_p = c/K$ constitutes the passive current density. This formulation can represent the observable characteristics of the active-passive transition as demonstrated in a previous paper.¹⁹

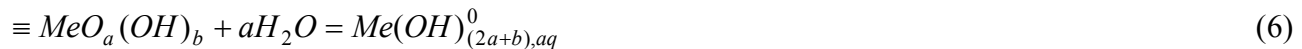
For calculating the corrosion potential, the quantitative modeling of passive dissolution is of primary importance. In the absence of specific active ions, the passive current density depends primarily on the pH of the solution. For acidic solutions, we consider a dissolution reaction between the passive oxide/hydroxide surface layers and protons from the solution, i.e.



where the symbol “ \equiv ” denotes surface species. The corresponding kinetic equation is

$$i_{p,H^+} = k_{H^+} a_{H^+}^{*s} \quad (5)$$

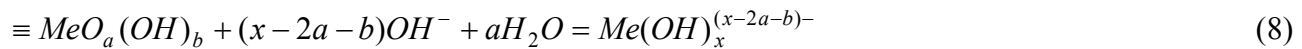
where $a_{H^+}^{*s}$ denotes the surface concentration of hydrogen ions and s is a reaction order, which is not necessarily related to the stoichiometric coefficient in the dissolution reaction. In neutral solutions, the predominant dissolution reaction is:



where the predominant species on the right-hand side of eq. (10) is a neutral complex as indicated by the superscript 0. The corresponding kinetic equation is:

$$i_{p,H_2O} = k_{H_2O} a_{H_2O}^{*u} \quad (7)$$

where the reaction order with respect to water indicates that dissolution may be affected by water activity. Similarly, the predominant reaction in alkaline solutions is



with a corresponding kinetic equation given by

$$i_{p,OH^-} = k_{OH^-} a_{OH^-}^{*v} \quad (9)$$

The total passive current density as a function of pH is given by

$$i_p = i_{p,H^+} + i_{p,H_2O} + i_{p,OH^-} \quad (10)$$

The kinetic equations can be rewritten in terms of bulk concentrations of ions by considering the mass transfer equation:

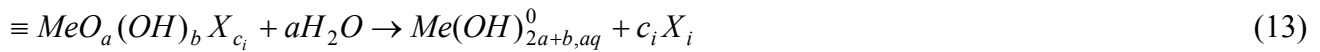
$$\frac{i_{p,i}}{zF} = k_m (a_i - a_i^*) \quad (11)$$

where k_m is a mass transfer coefficient and a_i is the bulk activity of the reacting species. The mass transfer coefficient can be computed for various flow regimes as described in a previous paper.¹⁸ Then, the surface concentration a_i^* can be obtained from eq. (11) and substituted into eq. (5), (7) or (9).

In addition to pH effects, some active ions may influence the magnitude of the passive current density. The effect of active species on the dissolution in the passive state can be modeled by considering surface reactions between the metal oxide film and solution species, i.e.,



where X_i is the i -th reactive species in the solution and the subscripts a , b , c_i and e_i represent the reaction stoichiometry. In eq. (12), the stoichiometry is usually difficult to define because of the dynamic nature of the system and may be, in general, fractional. In general, eq. (12) may be written for any active, aggressive or inhibitive, species i in the solution ($i = 1, \dots, n$). It is reasonable to assume that eq. (12) is in quasi-equilibrium and characterize it by an equilibrium constant. The surface species that forms as a result of reaction (12) may undergo irreversible dissolution reactions such as



in which dissolved metal species are formed in analogy to those described by eqs. (4), (6) and (8). Mathematical analysis of reactions (12-13)¹⁸⁻¹⁹ yields a relationship between the passive current density and activities of reactive species, i.e.,

$$i_p = i_p^0(pH) \frac{1 + \sum_i l_i \frac{a_{X_i}^{c_i}}{a_{OH^-}^{e_i}}}{1 + \sum_i K_i \frac{a_{X_i}^{c_i}}{a_{OH^-}^{e_i}}} \quad (14)$$

where $i_p^0(pH)$ is given by eq. (10), l_i is the forward rate of reaction (15) and K_i is the equilibrium constant of reaction (12).

Typical cathodic processes may include the reduction of dissolved oxygen, water molecules, protons, various transition metal cations (e.g., ferric, cupric) and various anions that can be reduced in electrochemical reactions (e.g., nitrates, nitrites, chromates, vanadates, etc.) A generic cathodic process may be written as a reduction reaction of an electrochemically active species X :



Cathodic processes are often subject to mass-transfer limitations, due to the diffusion of dissolved molecules to the metal surface. Thus, an expression for the current density for reaction (15) takes the form

$$\frac{1}{i_X} = \frac{1}{i_{X,a}} + \frac{1}{i_{X,\text{lim}}} \quad (16)$$

where the activation-controlled term is given by

$$i_{X,a} = i_X^* a_X^q a_{H^+}^r \exp\left[\frac{-\alpha_X F(E - E_X^0)}{RT}\right] \quad (17)$$

and the limiting current density for the reduction of X is

$$i_{X,\text{lim}} = b k_m F a_X \quad (18)$$

Examples of various specific cathodic processes were discussed in previous papers.^{19,20} The reaction orders q and r in eq. (17) are, in general, specific to the metal surface although they are similar within families of alloys (especially for alloys from the Fe-Ni-Cr-Mo family). On the other hand, the diffusion-limited current density (eq. 18) is practically independent of the surface because the mass-transfer coefficient depends only on flow conditions, diffusivity of species X and density and viscosity of the solution. In this study, the reaction orders are determined from experimental data and the limiting current densities are predicted for simple single-phase flow regimes as described in previous papers.^{18,19} Thus, the limiting current densities are not adjusted using experimental data. For the calculation of the corrosion potential on stainless steels and nickel-base alloys, eq. (17) plays the most important role since reduction of redox species on passive surfaces usually does not proceed under mass transfer control. Eq. (17) is treated as a semi-empirical expression in which the constant i_X^* and the reaction orders q and r are calibrated to match experimental data.

The parameters of the electrochemical model are determined by utilizing a large number of experimental polarization and corrosion rate data. The partial electrochemical processes described above are combined into a total predicted polarization curve. Then, the corrosion potential is calculated by applying the mixed-potential theory, i.e.,

$$\sum i_{c,i} = \sum i_{a,j} \quad (19)$$

where $i_{c,i}$ and $i_{a,j}$ denote the i -th cathodic and j -th anodic process. The electrochemical parameters of the model are determined in a multi-step procedure, i.e.,

1. The kinetic rate constants for calculating the passive current density (eq. 10) are obtained from experimental current densities for passive dissolution as a function of pH;
2. The exchange current density and electrochemical transfer coefficient for anodic dissolution of the metal in the active state (eq. 1) are obtained from corrosion rate data and polarization curves for the active dissolution in acidic environments.
3. The exchange current density and electrochemical transfer coefficient for the reduction of water molecules (eqs. 15-17 for $X = \text{H}_2\text{O}$) are obtained from corrosion potential measurements and cathodic polarization curves in deaerated solutions. These parameters are necessary to establish a baseline for systems that do not contain specific redox components.
4. The exchange current density and electrochemical transfer coefficient for the reduction of hydrogen ions (eqs. 15-17 for $X = \text{H}^+$) are determined from corrosion rate data in acidic solutions.
5. For the reduction of oxygen molecules (eqs. 15-17 for $X = \text{O}_2$), the exchange current density, reaction order with respect to dissolved oxygen and electrochemical transfer coefficient are

established on the basis of corrosion potential data and cathodic polarization curves in solutions with various levels of dissolved oxygen.

6. Similarly, analogous parameters for the reduction of other oxidants are obtained from corrosion potential data in solutions containing various concentrations of oxidants.

Modeling the repassivation potential

In a previous paper (Anderko et al.¹⁵), a comprehensive model has been developed for calculating the repassivation potential of alloys as a function of solution chemistry and temperature. Further, the model has been shown to be accurate for representing the effects of aggressive, non-aggressive and inhibitive species on the repassivation potential. Here, we briefly outline the fundamental concepts of this model and its parameters.

The repassivation potential model considers the electrochemistry of a metal M that undergoes dissolution underneath a layer of concentrated metal halide solution MX. The concentrated solution may or may not be saturated with respect to a hydrous solid metal halide. The thickness of the hydrous halide layer is assumed to be much smaller than the size of the pit so that the system may be regarded as one-dimensional. In the process of repassivation, a thin layer of oxide forms at the interface between the metal and the hydrous metal halide. The model assumes that, at a given instant, the oxide layer covers a certain fraction of the metal surface. This fraction increases as repassivation is approached. Further, the model includes the effects of multiple aggressive and non-aggressive or inhibitive species, which are taken into account through a competitive adsorption scheme. The aggressive species form metal complexes, which dissolve in the active state. On the other hand, the inhibitive species and water contribute to the formation of oxides, which induce passivity. In general, the equations that describe these processes are complex and can be solved only numerically. However, a closed-form equation has been found in the limit of repassivation, i.e., when the current density reaches a predetermined low value i_{rp} (typically $i_{rp} = 10^{-2}$ A/m²) and the fluxes of metal ion become small and comparable to those for passive dissolution. This closed-form expression, which can be solved to calculate the repassivation potential, is given by:

$$1 + \sum_j \left[\left(\frac{i_{rp}}{i_p} - 1 \right) \frac{l_j''}{i_{rp}} \right] \theta_j^{n_j} \exp\left(\frac{\xi_j F E_{rp}}{RT} \right) = \sum_j \frac{k_j''}{i_{rp}} \theta_j^{n_j} \exp\left(\frac{\alpha_j F E_{rp}}{RT} \right) \quad (20)$$

where E_{rp} is the repassivation potential, i_p is the passive current density, T is the temperature, R is the gas constant and F is the Faraday constant. The partial coverage fraction of a species j is related to the activity of this species in the bulk solution by

$$\theta_j = \frac{r_j a_j}{1 + \sum_k r_k a_k} \quad (21)$$

Eq. (20) contains the following parameters:

- (1) Scaled rate constant for aggressive ions, which can be expressed using a scaled Gibbs energy of activation $\Delta g_{A,j}^\ddagger$:

$$k_j = \frac{k_j''}{i_{rp}} = \exp\left(-\frac{\Delta g_{A,j}^\ddagger}{RT} \right) \quad (22)$$

(2) Scaled rate constant for inhibitive species, which is also expressed using a scaled Gibbs energy of activation $\Delta g_{I,j}^\ddagger$:

$$\left(\frac{i_{rp}}{i_p} - 1\right) \frac{l_j''}{c} = \exp\left(-\frac{\Delta g_{I,j}^\ddagger}{RT}\right) \quad (23)$$

(3) Reaction order with respect to aggressive ions, n_j ;

(4) Electrochemical transfer coefficients for the inhibitive species, ξ_j ;

(5) Scaled Gibbs energy of adsorption $\Delta G_{ads,i}$, which defines the adsorption coefficient in eq. (21):

$$r_j = \exp\left(-\frac{\Delta G_{ads,j}}{RT}\right) \quad (24)$$

However, the latter property can be assigned a common default value for almost all species.

The scaled Gibbs energies of activation may be further related to temperature as

$$\frac{\Delta g_{A,j}^\ddagger}{T} = \frac{\Delta g_{A,j}^\ddagger(T_{ref})}{T_{ref}} + \Delta h_{A,j}^\ddagger \left(\frac{1}{T} - \frac{1}{T_{ref}}\right) \quad (25)$$

and

$$\frac{\Delta g_{I,j}^\ddagger}{T} = \frac{\Delta g_{I,j}^\ddagger(T_{ref})}{T_{ref}} + \Delta h_{I,j}^\ddagger \left(\frac{1}{T} - \frac{1}{T_{ref}}\right) \quad (26)$$

Further, the electrochemical transfer coefficients for aggressive species (α_i) are assumed to be equal to one and the reaction orders for the effects of inhibiting species (n_j) can be assigned a default value.¹⁴

The parameters of the repassivation potential model are typically determined as follows:

- (1) Since E_{rp} data are most abundant for chloride solutions, the scaled rate constant for the chloride ions ($\Delta g_{A,Cl}^\ddagger$), reaction order with respect to chlorides (n_{Cl}), scaled rate constant for water ($\Delta g_{I,H_2O}^\ddagger$), and electrochemical transfer coefficient for water (ξ_{H_2O}) are determined based on data for chloride solutions. As discussed in a previous paper,¹⁴ this procedure can be simplified by the fact that the n_{Cl} and ξ_{H_2O} parameters have universal values for Fe-Ni-Cr-Mo-W alloys and do not need to be individually determined. If the temperature range of the data is sufficient to establish the temperature dependence, $\Delta h_{A,Cl}^\ddagger$ and $\Delta h_{I,H_2O}^\ddagger$ may also be determined.
- (2) The $\Delta g_{A,j}^\ddagger$ and, if necessary, n_j parameters are determined for other aggressive species j (e.g., bromide ions) using E_{rp} data for either pure or mixed solutions containing such ions.
- (3) The $\Delta g_{I,k}^\ddagger$ parameters for inhibitive ions k are determined on the basis of data for mixed solutions containing chlorides and inhibitors. Data for mixed systems are necessary because E_{rp} is undefined in solutions containing only inhibitors.

RESULTS AND DISCUSSION

Calculation of corrosion potential and corrosion rates

The general corrosion model described above is capable of simultaneously representing the corrosion potential and corrosion rates. Although corrosion potential is of primary interest for localized corrosion, simultaneous representation of the corrosion potential and corrosion rates ensures that the parameters of the electrochemical model are meaningful over wide ranges of condition. Also, the rates of general corrosion are of significant practical significance, primarily in the acidic range.

In this study, the model has been first applied to nickel-base alloys in acid mixtures. Figures 2 and 3 show the corrosion rates of alloy 276 (UNS N10276) in aqueous solutions of nitric acid and sulfuric acid, respectively. In both figures, the calculated rates are plotted as functions of acid concentration at several temperatures and compared with experimental data obtained from multiple sources. As described above, the parameters of the electrochemical model were calibrated using experimental data for the alloy in pure acids. Then, the parameters were used to predict corrosion rates in mixed $\text{HNO}_3 - \text{H}_2\text{SO}_4 - \text{H}_2\text{O}$ solutions. As shown in Figure 4, the rates in the mixed system are predicted with very good accuracy, which indicates that the parameters of the electrochemical model are internally consistent.

Figure 5 shows the calculated and experimental corrosion potentials for alloy 22 (UNS N06022) in the mixed system $\text{HNO}_3 - \text{HCl} - \text{H}_2\text{O}$. A strong increase in the corrosion potential is observed as nitric acid is added to hydrochloric acid solutions. This increase is due to the change in the dominant cathodic reaction. In HCl solutions, the dominant cathodic reaction is the reduction of protons, which occurs in the active state at sufficiently high acid concentration (i.e., for pH values below the depassivation pH). This corresponds to low corrosion potentials as shown in Figure 5 for $m(\text{HNO}_3) = 0$. In the presence of sufficient concentrations of nitric acid, reduction of nitrate ions or undissociated HNO_3 molecules becomes the dominant cathodic reaction. This strongly increases the corrosion potential. The model correctly reproduces this phenomenon as shown in Figure 5. It should be noted that only the data for HCl and HNO_3 were used to calibrate the model parameters.

To perform a more detailed analysis of the effect of nitrates on the corrosion potential, a number of E_{corr} measurements have been obtained in this study as a function of pH. To ensure that the pH effect is reproducible, the solutions were prepared in three alternative ways, i.e., by using 0.5 M NaNO_3 and adjusting pH with H_2SO_4 or by using 0.4 M $\text{NaNO}_3 + 0.1$ M HNO_3 and varying pH with H_2SO_4 or by adjusting the relative proportions of NaNO_3 and HNO_3 to maintain the total concentration of NO_3 equal to 0.5 M while varying the pH (cf. Figure 6). In all cases, 0.5 M Na_2SO_4 was used as background electrolyte. The solution was purged with nitrogen and the final dissolved oxygen concentration was determined to vary from ca. 0.15 ppm to 1.6 ppm. As expected, model calculations have revealed that the predicted corrosion potential is not sensitive to the procedure that was used to adjust the pH of the solution. However, a strong sensitivity to dissolved oxygen concentration has been determined. To illustrate this, Figure 6 shows calculated corrosion potentials for two assumed dissolved oxygen concentrations, i.e., 1.2 ppm (thick line) and 0.12 ppm (thin line). It is noteworthy that the corrosion potential does not depend on dissolved oxygen concentration in strongly acidic solutions (i.e., at $\text{pH} = 0 \sim 0.5$). This is due to the fact that, at high acidity, reduction of nitric acid plays a dominant role and is not affected by oxygen concentration. At higher pH values, both the reduction of nitric acid and oxygen contribute to the corrosion potential. The scattering of experimental data in Figure 6 is explained by the variations in dissolved oxygen concentration. The calculated corrosion potentials bracket the experimental data once the variations in dissolved oxygen concentration are taken into account.

Additional analysis of the effect of oxygen on the corrosion potential of alloy 22 (UNS N06022) is shown in Figure 7. In this case, the solutions were aerated at various temperatures and the effect of pH

was investigated. As shown in Figure 7, pH and temperature are the primary variables that determine the corrosion potential in this case. The pH effect is particularly pronounced in acidic solutions. On the other hand, the effect of chlorides is negligible. These effects are accurately represented by the model.

As described above, the general corrosion model relies on the detailed treatment of partial electrochemical processes on the metal surface. Therefore, it predicts a current density (i) versus potential (E) relationship, which is consistent with the observed corrosion rates and potentials. Such a predicted i vs. E relationship can be used to rationalize the relative importance of various electrochemical reactions. This is illustrated in Figure 8, which details the partial electrochemical processes in nitrate systems at pH=0 (upper diagram) and pH=3 (lower diagram). In both cases, the conditions are the same as those described in Figure 6. In Figure 8, the dotted lines illustrate the partial electrochemical reactions whereas the solid line shows the total predicted polarization curve. At pH=0, the dominant cathodic reactions are the reduction of NO_3^- ions (denoted by “4” in Figure 8) and the reduction of HNO_3^0 molecules (denoted by “5”). Reduction of oxygen molecules (denoted by “3”) is insignificant compared to these reactions. Therefore, the corrosion potential is not affected by dissolved oxygen concentration at pH=0. On the other hand, reduction of oxygen molecules becomes the predominant cathodic reaction at pH=3. This is consistent with the sensitivity of E_{corr} to dissolved oxygen concentration (cf. Fig. 6).

Another important class of redox species are the transition metal cations. In particular, ferric and cupric ions are used for standardized localized corrosion testing to obtain the critical pitting and crevice temperatures. In a previous paper,²⁴ the effect of concentration of redox species was studied. Here, we focus on E_{corr} in relatively concentrated solutions of ferric and cupric ions as a function of temperature. The results of calculations for alloy 22 (UNS N06022) are shown in Figure 9 and compared with corrosion potentials in hydrogen-purged acidic solutions. In all cases, good agreement with experimental data has been obtained.

Calculation of the repassivation potential

In a previous paper,¹⁵ it has been demonstrated that the repassivation potential model can reproduce E_{rp} data for alloys in solutions containing aggressive, non-aggressive and inhibitive ions. Furthermore, it has been shown¹⁴ that the parameters of the model can be correlated with alloy composition for chloride solutions. This correlation has a substantial practical significance because it makes it possible to predict the repassivation potential in chloride solutions for alloys from the Fe-Ni-Cr-Mo-W-N family for which no experimental data are available.

In this study, we focus on extending this correlation to systems that may contain other species in addition to chlorides. While chlorides are the most ubiquitous aggressive species, there are many species that may act as inhibitors and dramatically affect the repassivation potential and, hence, the tendency for localized corrosion. In the first step, we focus on the effect of nitrates because a substantial database exists for the effect of nitrates on the repassivation potential. Relatively complete data are available for alloys N06022 and N06690 and type 316L stainless steel (S31603). Also, fragmentary data exist for alloys 625 (UNS N06625), 800 (UNS N08800), 254SMO (S31254) and super-13 Cr stainless steel (S41425).

As described above, the effect of an inhibitor on the repassivation potential is governed by three parameters, i.e., (1) the Gibbs energy of activation for the formation of oxide, mediated by the adsorption of the inhibitor I , $\Delta g_{I,j}^\ddagger$, (2) enthalpy of activation for the same reaction, $\Delta h_{I,j}^\ddagger$ and (3) the electrochemical transfer coefficient for inhibitive species, ξ_j . Analysis of the available experimental data has revealed that the $\Delta h_{I,\text{NO}_3}^\ddagger$ and ξ_{NO_3} parameters can be assigned constant values for all alloys. For

calculating the $\Delta g_{I,NO_3}^\ddagger$ parameter, it has been determined that a linear correlation exists between the Gibbs energies for the formation of oxide through the adsorption of water (which was previously determined on the basis of E_{rp} data in chloride solutions) and through the adsorption of nitrate, i.e.

$$\Delta g_{I,NO_3}^\ddagger = -21.16 + 1.11\Delta g_{I,H_2O}^\ddagger \quad (27)$$

The existence of such a correlation is understandable in view of the fact that the $\Delta g_{I,j}^\ddagger$ parameter measures the ease with which a metal surface can be passivated. If a given metal is relatively easily passivated through a reaction with water, then it is also easily passivated as a result of the presence of nitrates. Thus, both parameters should show the same trends with alloy composition, although their numerical values are very different. Figure 10 shows the prediction of the repassivation potential for four alloys when the parameters for nitrates are calculated from the correlation. These calculations have been made for mixed chloride + nitrate solutions in which the nitrate concentration is varied at fixed chloride concentrations. At a certain nitrate concentration (which depends on temperature and chloride concentration), the repassivation potential increases rapidly, which indicates complete inhibition of localized corrosion. As shown in Figure 10, the predicted values of the repassivation potential are in good agreement with experimental data.

Prediction of the critical crevice temperature

The corrosion potential and repassivation potential models can be used to predict the critical crevice temperature. At temperatures below CCT, the calculated corrosion potential (E_{corr}) should lie below the repassivation potential (E_{rp}) whereas it should exceed E_{rp} above CCT. Thus, the intersection of the E_{corr} and E_{rp} curves versus temperature provides an estimate of CCT. Thus, experimental critical crevice temperatures provide a stringent test of the accuracy of the E_{corr} and, in particular, the E_{rp} models. Figure 11 shows the dependence of the calculated corrosion and repassivation potentials on temperature for four nickel-base alloys (i.e., N10276, N06022, N06625, and N08825) in 6% $FeCl_3$ solutions. As shown in Figure 10, the repassivation potential shows the same qualitative behavior as a function of temperature with an initially steep decrease followed by a moderate decrease at higher temperatures. However, the exact temperature ranges that correspond to the high-slope and low-slope portions of the E_{rp} vs. T curve are strong functions of the localized corrosion resistance of the alloy. For more resistant alloys, the high-slope region lies at higher temperatures. On the other hand, the corrosion potential is similar for all three alloys because it establishes itself, in all cases, on fairly similar passive surfaces that are dominated by chromium oxides. Accordingly, alloy N06022 is shown to have the best resistance to localized corrosion in $FeCl_3$ solutions, alloy N08825 is the least resistant and alloys N10276 and N06625 show intermediate behavior. The intersection points of the E_{corr} and E_{rp} curves are in very good agreement, within the scattering of experimental data, with the experimental critical crevice temperatures obtained by Hibner²⁵ and Garner.²⁶

SUMMARY

General electrochemical models have been developed for calculating the corrosion potential and repassivation potential for various alloys in complex chemical environments. The corrosion potential is calculated from a mixed-potential model that combines comprehensive thermodynamic speciation calculations with a detailed treatment of partial electrochemical processes that may occur on the metal surface. The mixed-potential model has been verified by calculating corrosion rates in acids and corrosion potentials as a function of pH and concentration of oxidizing species. Furthermore, the mixed-potential model is useful for elucidating the interplay between various partial processes on the surface and, hence, it makes it possible to relate corrosion mechanisms to the observed corrosion rates and

corrosion potential. The repassivation potential is calculated from a separate model, which quantitatively considers competitive processes at metal/salt film/solution interfaces in the limit of repassivation. The E_{rp} model has been shown to be accurate for calculating the repassivation potential for mixtures containing both aggressive and inhibitive ions. When combined, the E_{corr} and E_{rp} models make it possible to predict the long-term occurrence of localized corrosion as a function of solution chemistry and temperature. This has been verified by successfully predicting the critical crevice temperature for four nickel-base alloys in $FeCl_3$ solutions. The models described here have been implemented in software that can be used to simulate both general and localized corrosion as a function of environmental variables.

ACKNOWLEDGEMENT

The work reported in this paper has been supported by the Department of Energy (award number DE-FC36-04GO14043) and co-sponsored by ChevronTexaco, DuPont, Haynes International, Mitsubishi Chemical, Shell, and Toyo Engineering.

REFERENCES

1. R.W. Staehle, B.F. Brown, J. Kruger, A. Agarwal (eds.), U.R. Evans Conference on Localized Corrosion, NACE-3, Houston, TX: NACE International, 1974.
2. Z. Szklarska-Smialowska, Pitting Corrosion of Metals, NACE International, Houston 1986.
3. H.S. Isaacs, U. Bertocci, J. Kruger and Z. Smialowska (eds.), Advances in Localized Corrosion, NACE-9, Houston, TX: NACE International, 1990.
4. P.M. Natishan, R.G. Kelly, G.S. Frankel and R.C. Newman (eds.), Critical Factors in Localized Corrosion, Pennington, NJ: The Electrochemical Society, 95-15, 1996.
5. P.M. Natishan, H.S. Isaacs, M. Janik-Czachor, V.A. Macagno, P. Marcus and M. Seo (eds.), Passivity and Its Breakdown, Pennington, NJ: The Electrochemical Society, 97-26, 1998.
6. M. Seo, B. Macdougall, H. Takahashi, and R.G. Kelly (eds.), Passivity and Its Breakdown, Pennington, NJ: The Electrochemical Society, 99-27, 1999.
7. C.Y. Chao, L.F. Lin, and D.D. Macdonald, *J. Electrochem. Soc.*, 128, 1187 (1981).
8. L.F. Lin, C.Y. Chao, and D.D. Macdonald, *J. Electrochem. Soc.*, 128, 1194 (1981).
9. D.E. Williams and Y.Y. Zhou, *J. Electrochem. Soc.*, 147, 1763 (2000).
10. J.W. Oldfield and W.H. Sutton, *Brit. Corrosion J.*, 13 (1978) 13.
11. S.M. Sharland, *Corrosion Sci.*, 33 (1992) 183.
12. S.M. Gravano and J.R. Galvele, *Corrosion Sci.*, 24 (1984) 517.

13. M. Watson and J. Postlethwaite, *Corrosion*, 46 (1990) 522.
14. A. Anderko, N. Sridhar, C.S. Brossia and D.S. Dunn, paper no. 04061, CORROSION/2004, New Orleans, LA (2004).
15. A. Anderko, N. Sridhar, and D.S. Dunn, *Corrosion Sci.*, 46 (2004) 1583.
16. D.S. Dunn, N. Sridhar, and G.A. Cragolino, *Corrosion*, 52 (1996) 115.
17. D.S. Dunn, G.A. Cragolino, and N. Sridhar, *Corrosion*, 56 (2000) 90.
18. A. Anderko and R.D. Young, *Corrosion*, 56 (2000) 543.
19. A. Anderko, P. McKenzie and R.D. Young, *Corrosion*, 57 (2001) 202.
20. N. Sridhar, C.S. Brossia, D.S. Dunn and A. Anderko, *Corrosion*, 60 (2004) 915-936.
21. M. Rafal, J. W. Berthold, N. C. Scrivner, S. L. Grise, Models for electrolyte solutions, in S. I. Sandler, ed., *Models for Thermodynamic and Phase Equilibria Calculations*, p. 601-670 (New York, NY: M. Dekker, 1995).
22. A. Anderko and M. M. Lencka, *Ind. Eng. Chem. Res.*, 37 (1998): p. 2878.
23. M.M. Lencka, A. Anderko, S.J. Sanders and R. D. Young, *Int. J. Thermophysics*, 19 (1998): p. 367.
24. C.S. Brossia, A. Anderko and N. Sridhar, paper no. 172, EUROCORR 2004, Nice, France (2004).
25. E.L. Hibner, CORROSION/86, paper no. 181, Houston, TX: NACE International (1986).
26. A. Garner, *Pulp and Paper Canada*, 82 (1981) 109.
27. ASM Handbook, Volume 13, *Corrosion*, ASM International (1987).
28. T.S. Lee III, and F.G. Hodge, *Mater. Performance* 15(9) (1976) 29.
29. Stellite Division, Cabot Corp., *Hastelloy Alloy C-276*, Publication F-30, 356D (1973).
30. R.C. Corbett, and W.S. Morrison, *Mater. Performance*, 56-59 (1989).
31. T.A. Mozhi, and R. Ray, *Materials Performance*, 29 (October), 50-54 (1990).
32. N. Sridhar, J.B.C.Wu and S.M.Corey, *Materials Performance* 26 (October), 17-23 (1987).
33. F.F. Berg, *Corrosion diagrams*, VDI - Verlag GmbH, D-4000 Dusseldorf, 1969.
34. W. Katz, *Casting in chemistry - the behavior of metallic cast materials under corrosive attack*, VDI - Verlag GmbH, D-4000 Dusseldorf.
35. Allegheny Ludlum Steel Corp., in *Handbook of Corrosion Data*, 2nd ed., ASME International, Materials Park, OH, 1995.

36. NACE Pub. 85-61573, "Corrosion in sulfuric acid," Proc. Corrosion/85, Symposium on corrosion in sulfuric acid, NACE, Houston, 1985.
37. Haynes International (1984), in Handbook of Corrosion Data, 2nd ed., ASME International, Materials Park, OH, 1995.
38. P.E. Manning and J.D. Schobel, Werkstoffe und Korrosion 37(3) (1986) 137.
39. F.T. McCurdy, Proc. Am. Soc. Testing Mater. 139 (1939) 698.
40. D.S. Dunn, L. Yang, Y.M. Pan, G.A. Cragnolino, CORROSION/2003, paper 3697, NACE International (2003).
41. J.C. Estill, G.A. Hust, R. Rebak, CORROSION/2003, paper 3688, NACE International (2003).
42. J. Kolts and N. Sridhar, Temperature Effect in Localized Corrosion, in Corrosion of Nickel Base Alloys, Proc. Int. Conf. on Nickel-Base Alloys, ed. By R.C. Scarberry, p. 191, ASM, 1984.

Table 1. Nominal compositions of alloys discussed in this paper

Name	UNS No.	Nominal Composition, weight percent					
		Ni	Fe	Cr	Mo	C	Others
Super 13Cr	S41425	5.9	Bal.	12.1	1.9	0.01	
alloy C-276	N10276	Bal.	5	15.5	16.0	0.01 max	W = 4
316L SS	S31603	10	Bal.	17.0	2.5	0.03 max.	
alloy 825	N08825	42	29	21.5	3.0	0.05 max	Cu = 2.0
alloy 625	N06625	Bal.	5 max	21.5	9.0	0.1 max	Nb = 3.65
alloy 22	N06022	56	3	22.0	13.0	0.01 max	W = 3.0
alloy 690	N06690	Bal.	9	29.0	0.0	0.05 max	

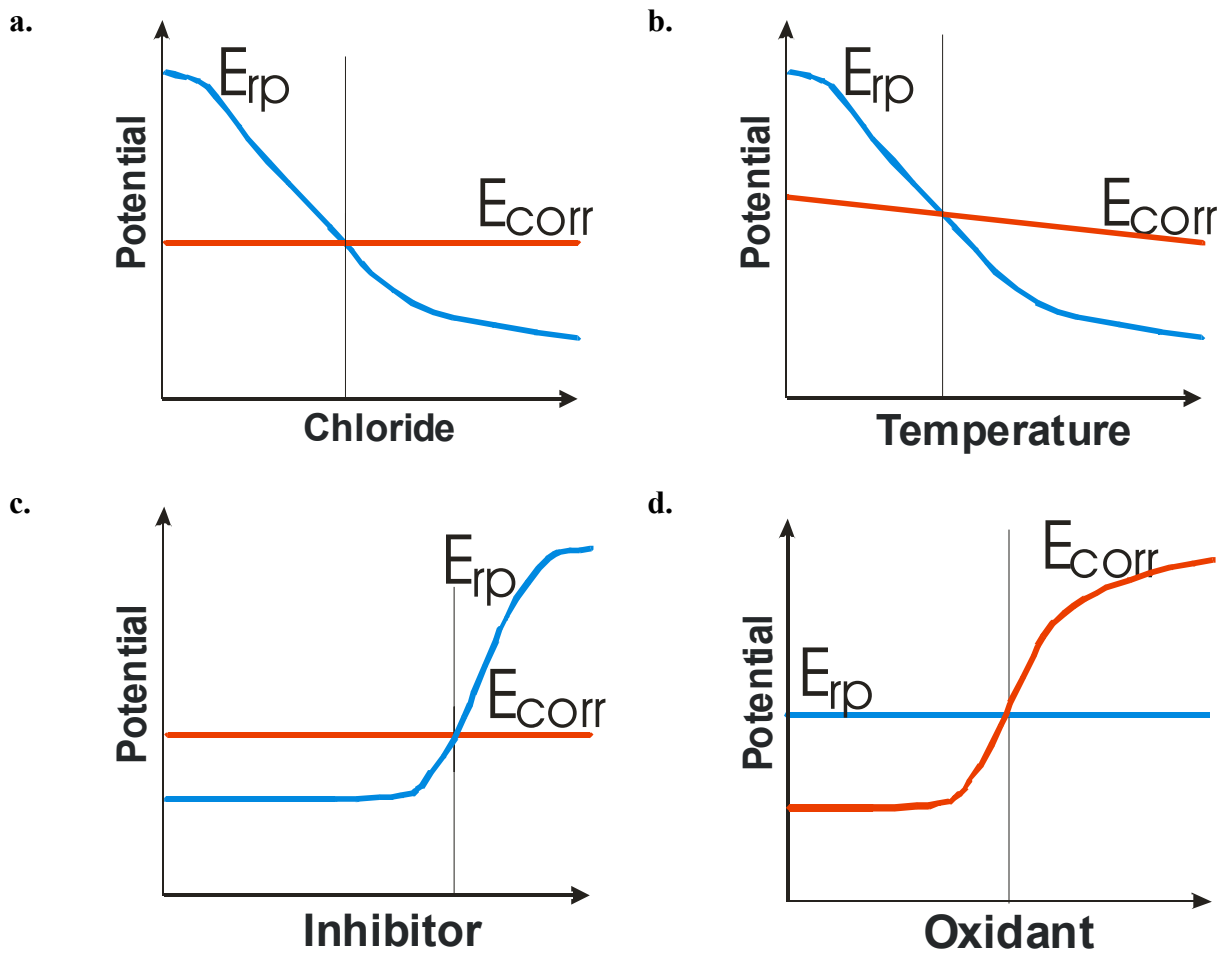


Figure 1. Schematic illustration of the relative behavior of the corrosion potential (E_{corr}) and repassivation potential (E_{rp}) as functions of different environmental variables.

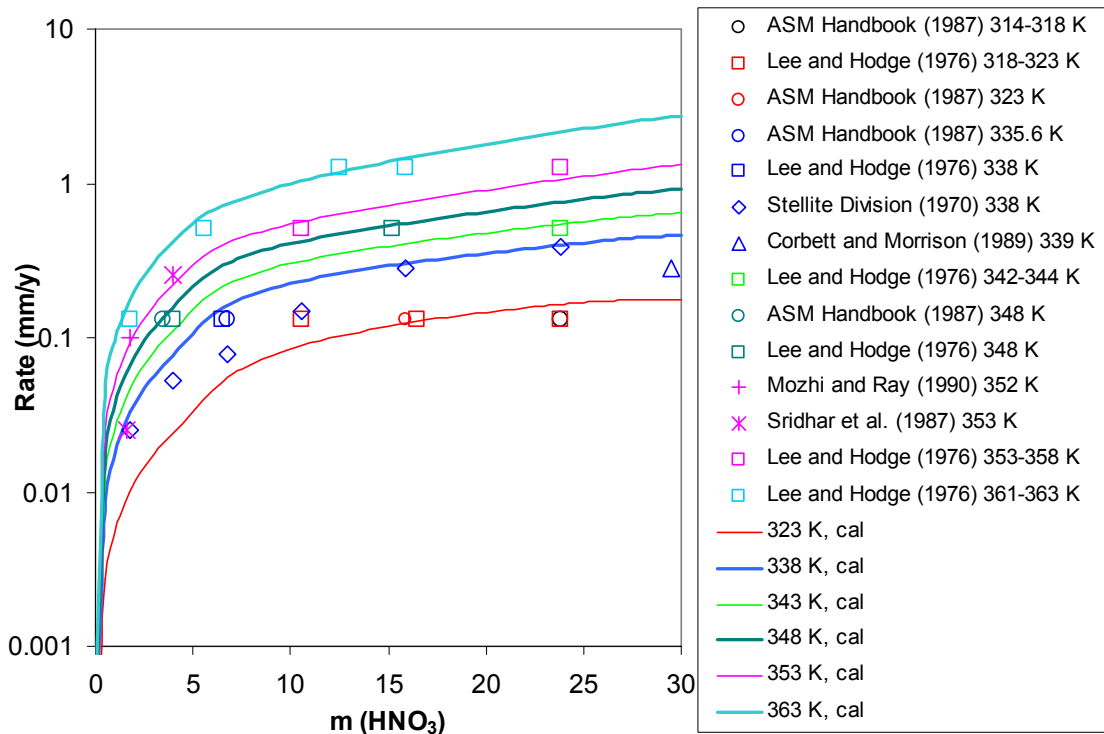


Figure 2. Calculated and experimental²⁷⁻³² corrosion rates of alloy C-276 in nitric acid as a function of acid concentration (in molality units, i.e., mol HNO₃ per 1 kg H₂O) at various temperatures.

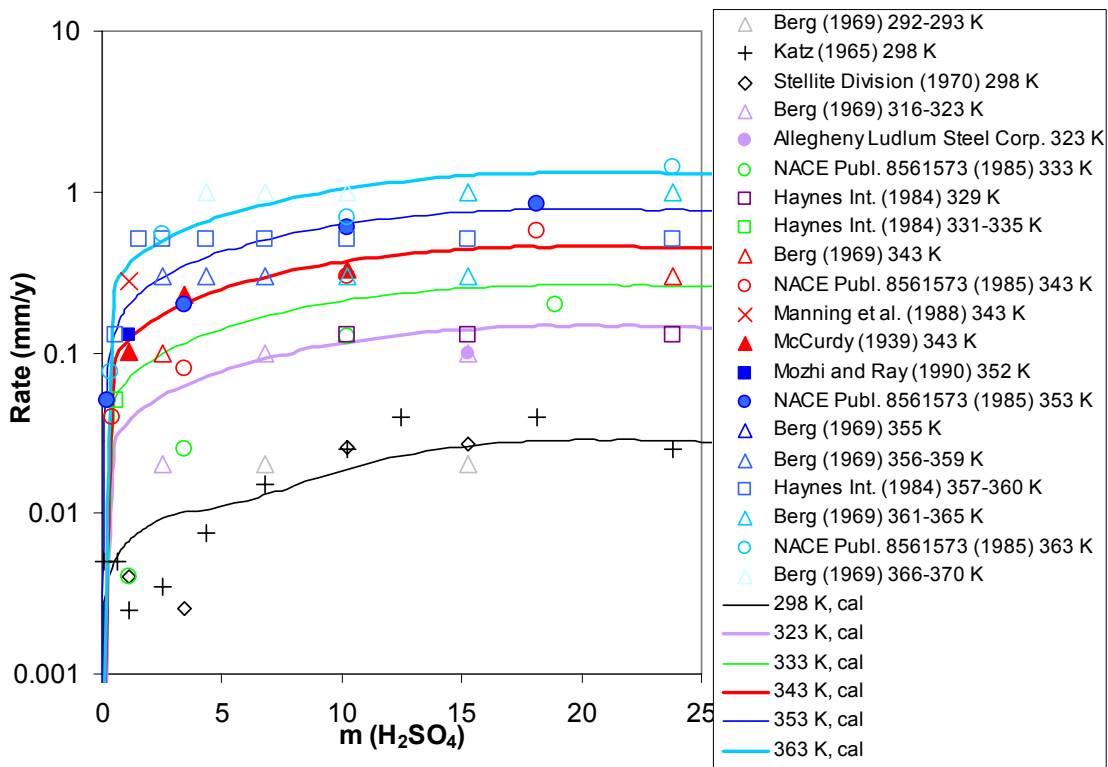


Figure 3. Calculated and experimental²⁹⁻³⁹ corrosion rates of alloy C-276 in sulfuric acid as a function of acid concentration (in mol per 1 kg H₂O) at various temperatures.

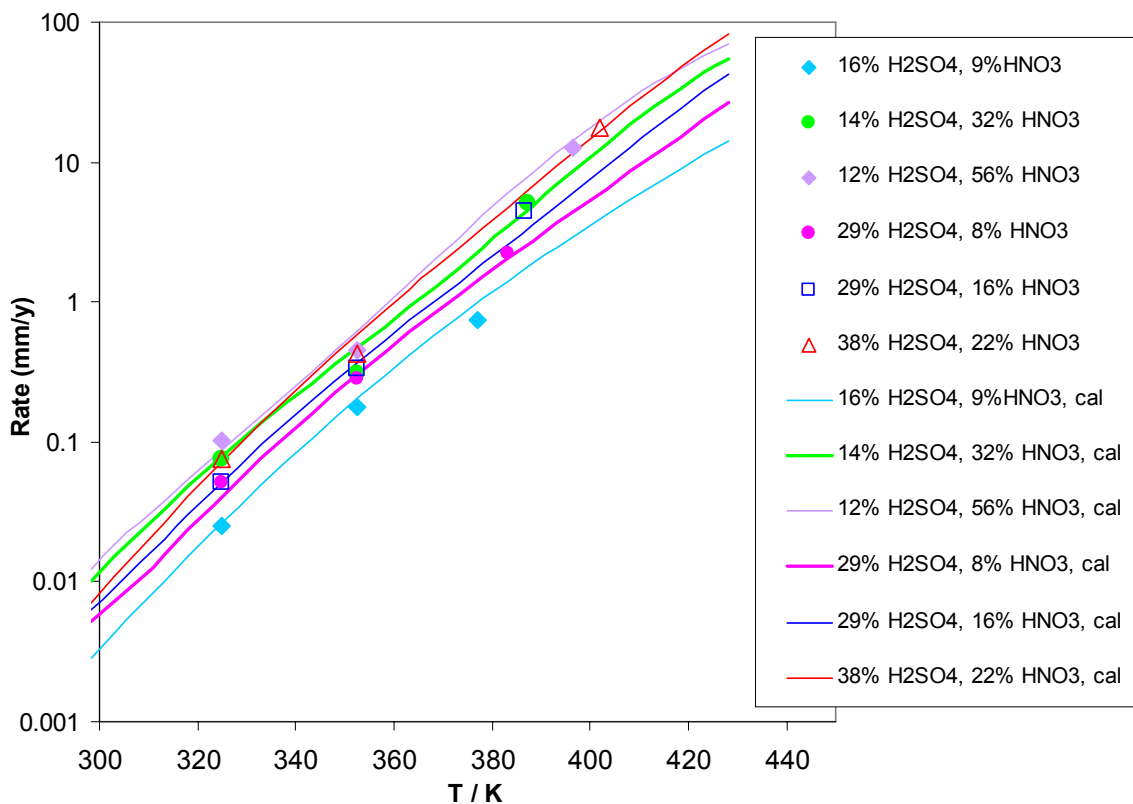


Figure 4. Prediction of corrosion rates of alloy C-276 in various $\text{H}_2\text{SO}_4 - \text{HNO}_3 - \text{H}_2\text{O}$ mixtures as a function of temperature.

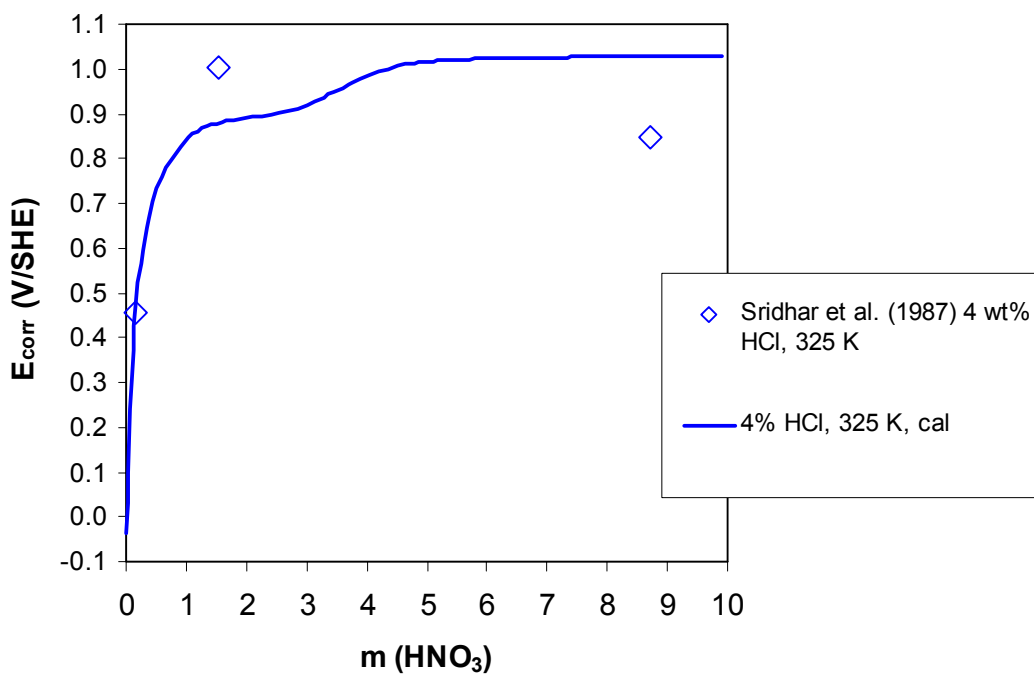


Figure 5. Calculated and experimental³² corrosion potentials of alloy C-22 in 4% HCl solutions with varying concentrations of HNO_3 .

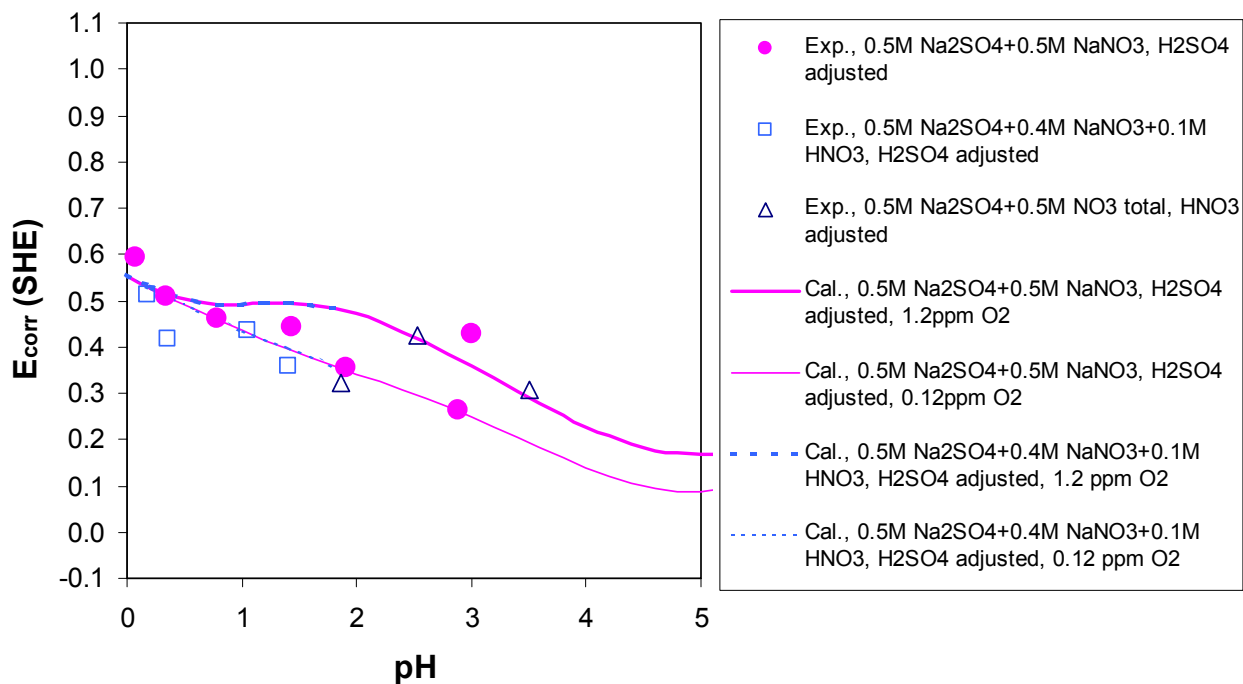


Figure 6. Calculated and experimental corrosion potentials of alloy C-22 as a function of pH in nitrate solutions with a total nitrate concentration of 0.5 M. Two different concentrations of dissolved oxygen (1.2 ppm and 0.12 ppm) have been assumed in the calculations.

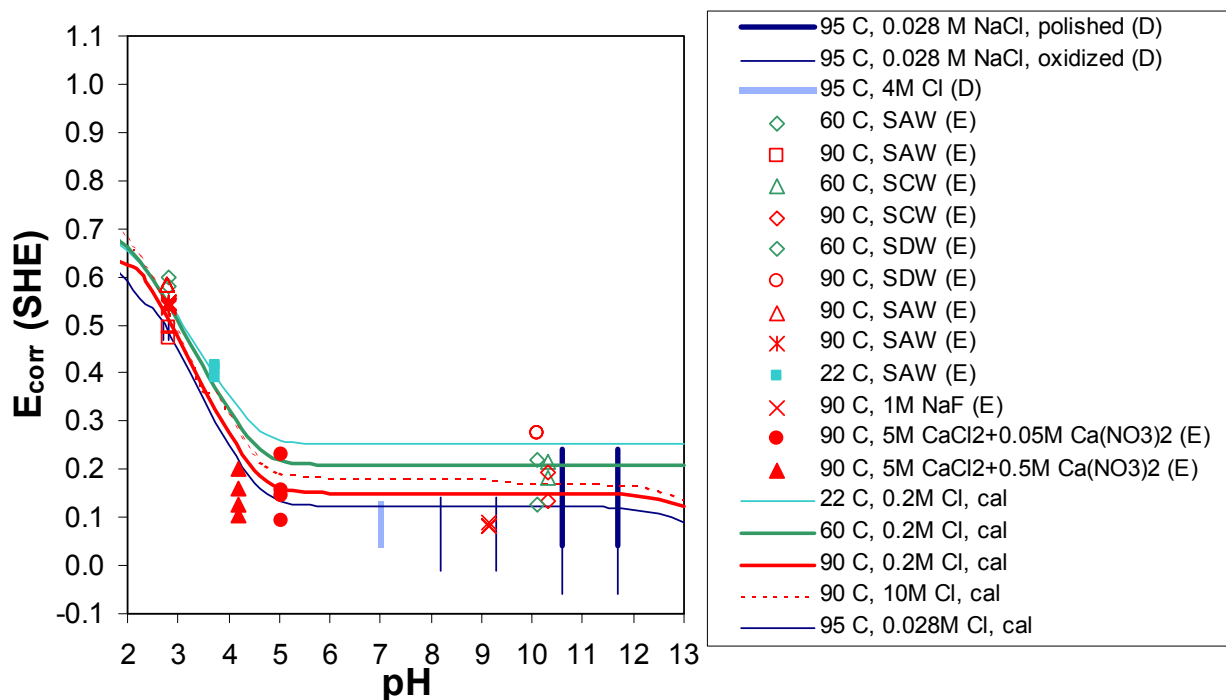


Figure 7. Calculated and experimental corrosion potentials for alloy C-22 in aerated waters as a function of pH. The symbols SAW, SCW and SDW denote simulated acidified water, simulated concentrated water and simulated dilute water, respectively. The data were taken from Dunn et al.⁴⁰ (D) and Estill et al.⁴¹ (E). The vertical lines show the ranges of data reported by Dunn et al.⁴⁰ for 0.028 M and 4 M NaCl solutions at 95 °C.

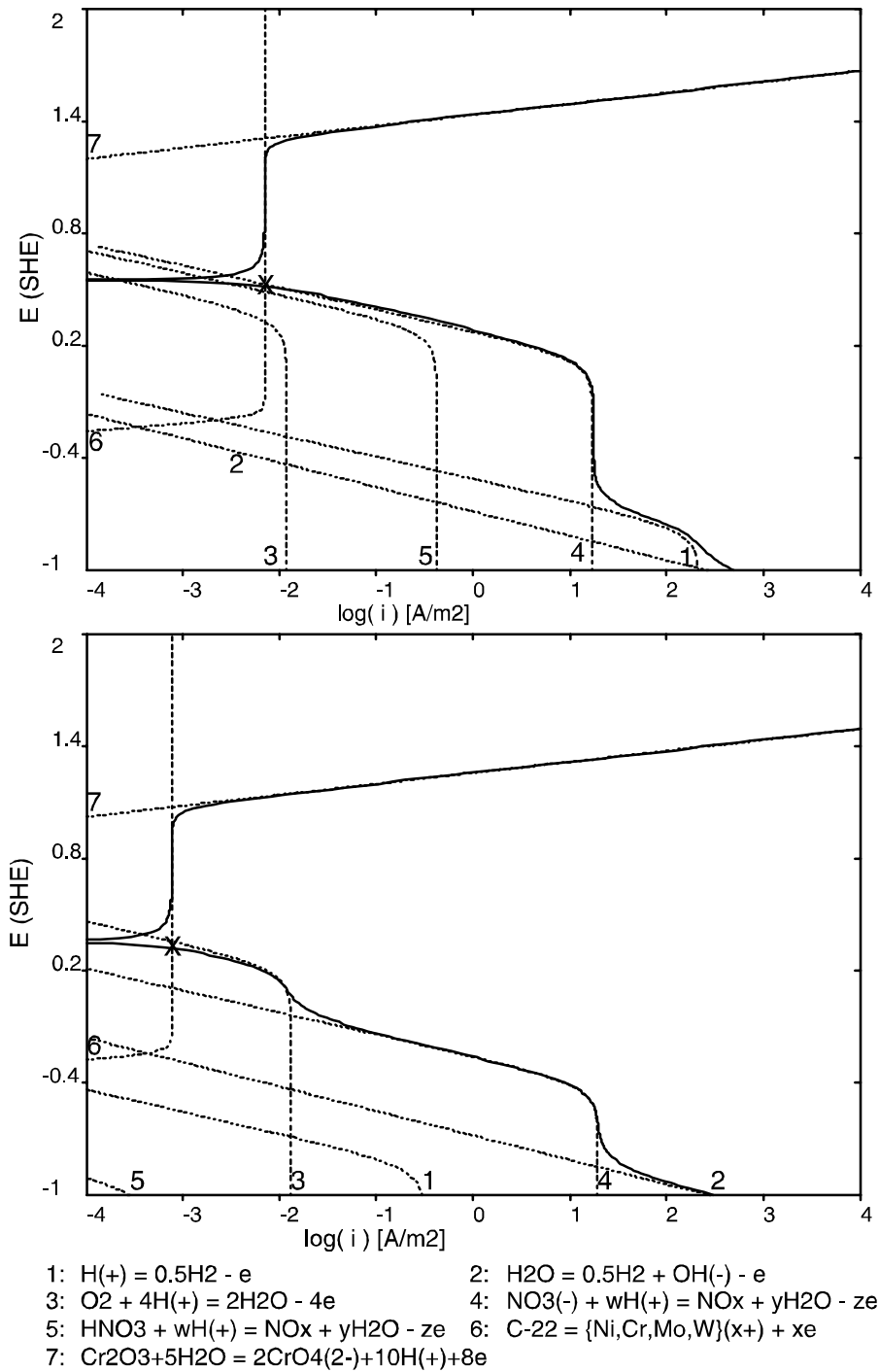


Figure 8. Calculated current density – potential relationship for alloy C-22 in a 0.5M NO_3^- - 0.5M SO_4^{2-} solution with pH = 0 (upper diagram) and pH=3 (lower diagram). In both cases, the dissolved oxygen concentration is 1.2 ppm. Partial electrochemical processes are shown as dotted lines and labeled with numbers, which are explained in the legend.

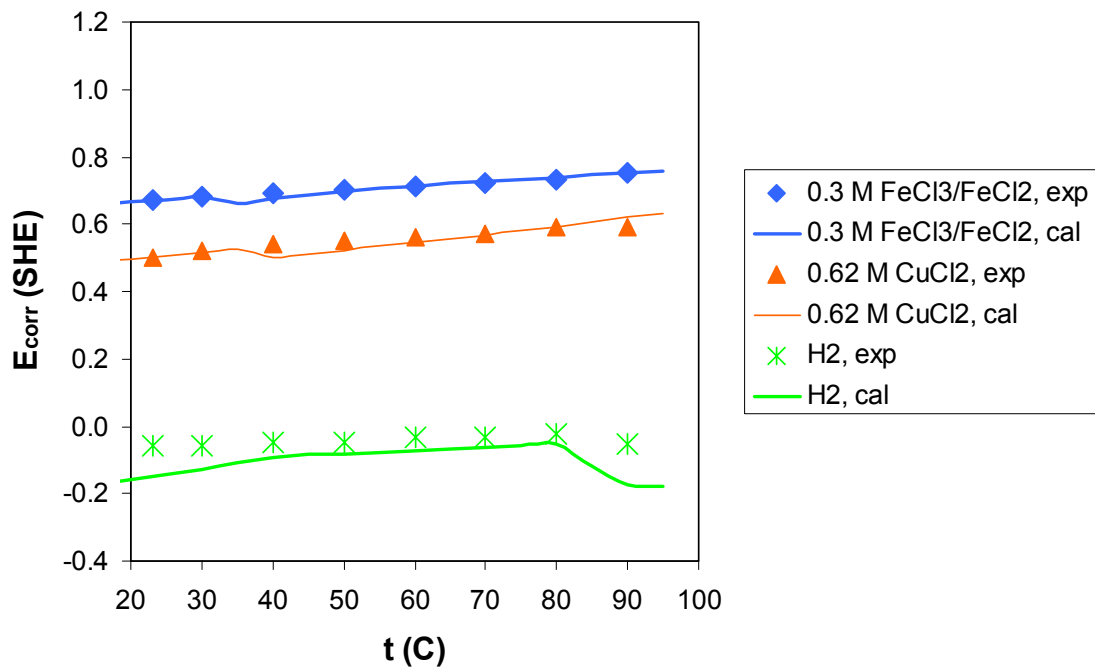


Figure 9. Calculated and experimental⁴² corrosion potentials for alloy C-22 in 0.3M FeCl₃/FeCl₂ solutions, 0.62M CuCl₂ solutions saturated with CuCl and H₂ – purged solutions with pH = 1.

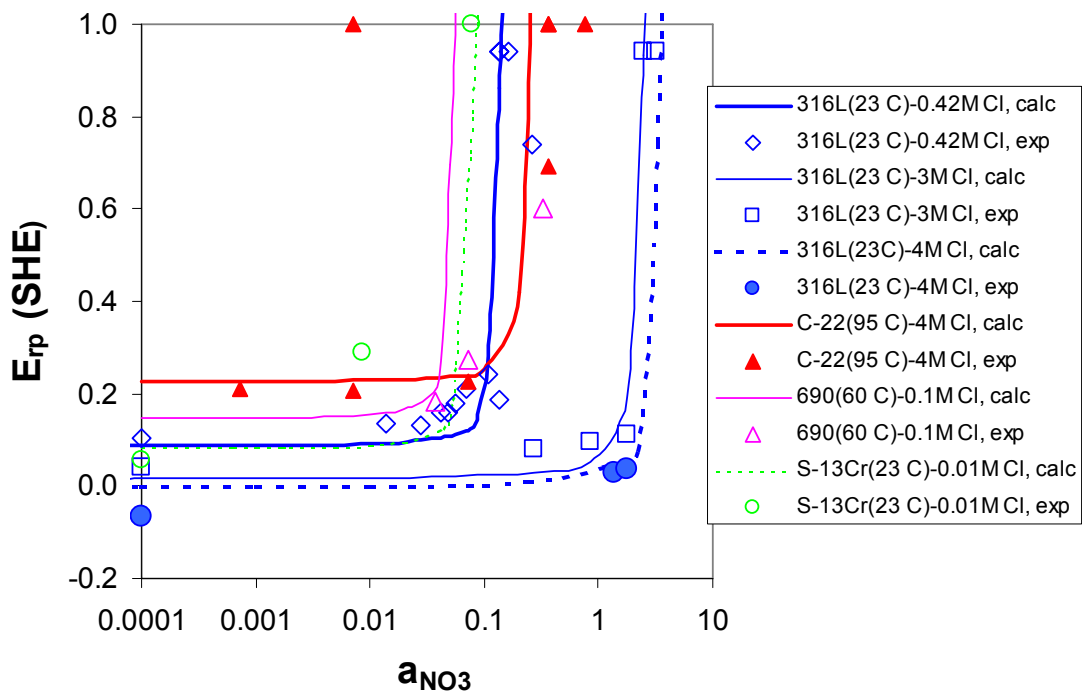
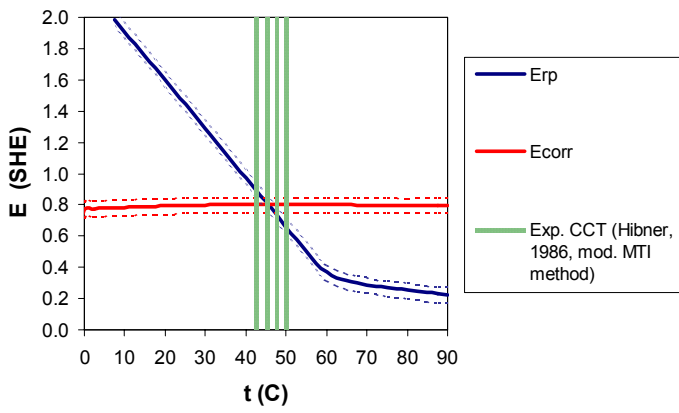
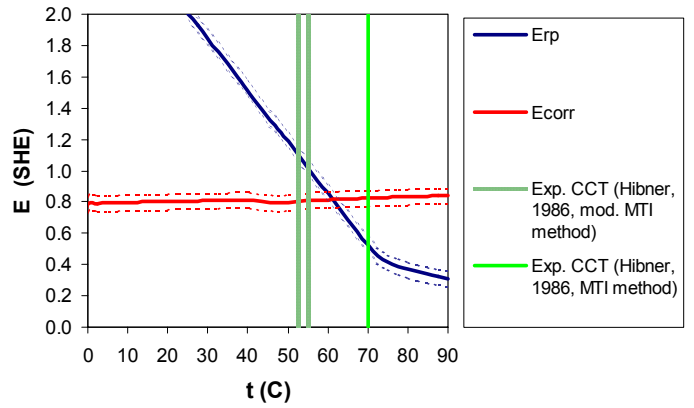


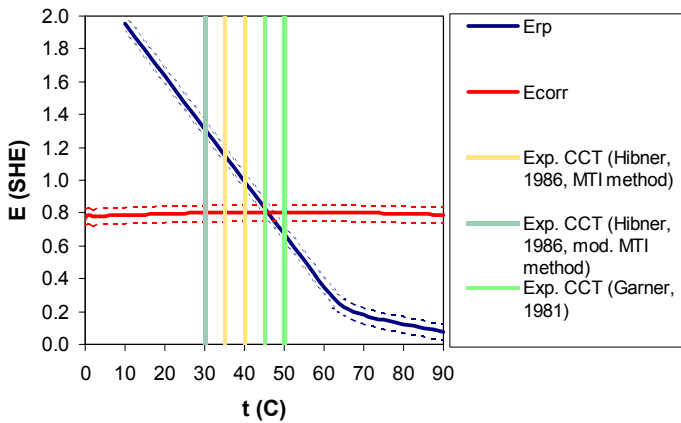
Figure 10. Calculated and experimental repassivation potentials for alloys 316L, C-22, 690 and super-13Cr in mixed chloride + nitrate solutions. The model parameters have been obtained from generalized correlations as a function of alloy composition.



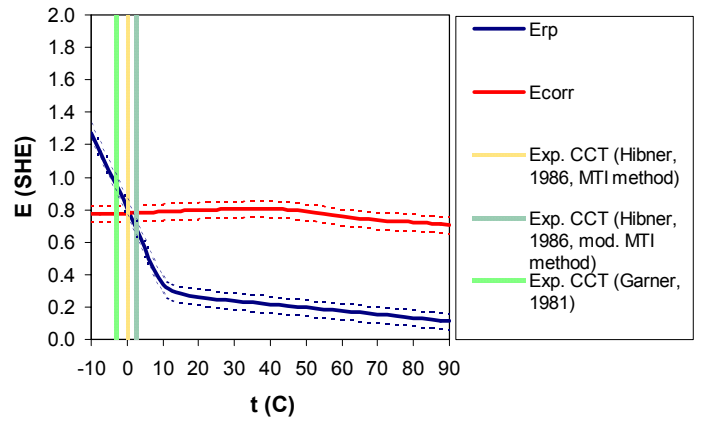
Alloy C-276



Alloy C-22



Alloy 625



Alloy 825

Figure 11. Prediction of the critical crevice temperature (CCT) for various alloys in a 6% FeCl₃ solution. The vertical lines show the location of the experimental CCT values.^{25,26} The intersection of the calculated corrosion potential and repassivation potential lines shows the predicted critical crevice temperature.